

# A MODIFIED WAVEMAKER BOUNDARY CONDITION FOR A NUMERICAL WAVE TANK BASED ON THE WCSPH METHOD

Amin Mahmoudi\*, Habib Hakimzadeh, Mohammad Javad Ketabdari, Hassan Abyan

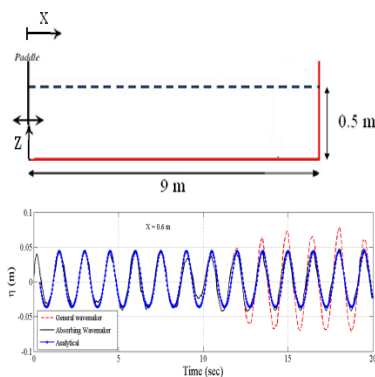
Hydraulic Structures, Persian Gulf University, Bushehr, Iran

## Article history

Received  
18 October 2015  
Received in revised form  
27 March 2016  
Accepted  
15 July 2016

\*Corresponding author  
a\_mahmoudi@pgu.ac.ir

## Graphical abstract



## Abstract

In this paper a space-averaged Navier–Stokes approach was deployed to Modified Wavemaker Boundary condition for a numerical wave tank. The developed model is based on the smoothed particle hydrodynamic (SPH) method which is a pure Lagrangian approach and can handle large deformations of the free surface with high accuracy. In this study, the large eddy simulation (LES) turbulent model was coupled with the weakly compressible version of the smoothed particle hydrodynamics (WCSPH) method to Modified Wavemaker Boundary condition for a numerical wave tank. An absorbing wavemaker boundary condition was developed to absorb the second reflecting waves from the wavemaker. The capacity of absorbing secondary reflecting waves and incoming waves in absorbing wavemaker was validated through comparisons of the numerical results with general wavemaker.

**Keywords:** WCSPH, wave reflection, absorbing wavemaker, numerical wave tank

© 2016 Penerbit UTM Press. All rights reserved

## 1.0 INTRODUCTION

The numerical wave flume is one of the main tools to research problems such as wave breaking and wave-structure interactions in coastal areas [1]. However, the multiple reflections of waves in traditional numerical flume reduce the accuracy and reliability of the model. Therefore, absorbing wavemaker and sponge layer are put forward to absorb the secondary reflecting waves from the wavemaker and the incident waves, respectively.

Liu and Zhao (1999) developed a numerical wave flume based on N-S equation and the finite-element method, in which the open boundary used Sommerfeld's radialization boundary conditions and artificial attenuation layer, and around the incident boundary, a speed attenuation region was set to absorb secondary reflected waves [2]. Shi *et al.* (2004) set up a numerical wave flume based on the Laplace equation and boundary element method, in which waves were made by the wave-making paddle, using Mitsuyasu Bretschneider spectrum as the control

signals, and the virtual wave absorbing and permeable layer were set at the open boundary [3]. Xu (2010) [4] and Omidvar *et al.* (2012) [5] used a sponge layer boundary condition to absorb the wave reflection from the wall at the end of the open channel based on the SPH method. Delavari *et al.* (2014) presented a modified sponge layer boundary condition for a numerical wave flume based on the SPH scheme [6].

In this paper, we use WCSPH method to develop a numerical wave flume similar to the physical wave flume. An absorbing wavemaker boundary condition is developed to absorb the second reflecting waves from the wavemaker. Afterwards, Regular waves are generated by the wave-making paddle and absorbed by the sponge layer at the end boundary. The capacity of absorbing second reflecting waves and incoming waves for absorbing wavemaker and sponge layer is validated through comparison of the numerical results with general wavemaker and solid boundary.

## 2.0 THE NUMERICAL MODEL

The continuity and Lagrangian form of N–S equations are as follows:

$$\frac{1}{\rho} \frac{d\rho}{dt} + \nabla \cdot \vec{u} = 0 \quad (1)$$

$$\frac{D\vec{u}}{Dt} = -\frac{1}{\rho} \nabla P + g + \nu_0 \nabla^2 \vec{u} + \frac{1}{\rho} \nabla \cdot \vec{\tau} \quad (2)$$

Where  $\rho$  is the density,  $t$  is the time,  $\vec{u}$  is the velocity,  $P$  is the pressure,  $g$  is the gravitational acceleration,  $\nu_0$  is the kinematic viscosity of laminar flow and  $\tau$  is the Reynolds stress.

### 2.1 The SPH Method

SPH is based on integral interpolants. The fundamental principle is to approximately obtain any function  $A(r)$  by (kernel approximation):

$$A(\vec{r}) = \int_{\Omega} A(\vec{r}') W(\vec{r} - \vec{r}', h) dr' \quad (3)$$

Where  $r$  is the vector position;  $W$  is the weighting function or kernel;  $h$  is called smoothing length. This estimation, in discrete notation, results in the following function (particle approximation):

$$A(r) = \sum_b m_b \frac{A_b}{\rho_b} W_{ab} \quad (4)$$

Where, the summation is over all the particles within the region of compact support of the kernel function. The mass and density are designate by  $m_b$  and  $\rho_b$  respectively and  $W_{ab} = W(\vec{r}_a - \vec{r}_b, h)$  is the weight function or kernel. SPH kernel approach offers an upside through calculating the derivative of a function analytically. This makes the method more accurate in comparison with a method like finite difference, where the derivatives are calculated from neighboring points using the spacing between them. For the irregularly spaced SPH particles, this would be extremely complicated. The derivatives of this interpolation can be obtained by ordinary differentiation .

$$\nabla A(r) = \sum_b m_b \frac{A_b}{\rho_b} W_{ab} \quad (5)$$

In the SPH conception, the motion of each particle is computed through interactions with the neighboring particles using an analytical kernel function. When the fluid is flowing, all terms in the N–S equations are formulated by particle interaction models and the need for a grid is obviated. SPH particles move in a Lagrangian coordinates and the advection in N–S equations is directly calculated by the particle motion without the numerical diffusion. Each particle can carry a mass  $m$ , velocity  $u$  and other properties would vary upon condition. The basic SPH formulations included in this study are summarized as follows [7].

The fluid in a standard SPH formulation is treated as compressible, allowing the use of an equation of state to determine fluid pressure, rather than solving another differential equation. However, the compressibility is adjusted to decelerate the speed of sound so that the time step in the model (based on the speed of sound) is reasonable. Changes in the fluid density are calculated as:

$$\frac{d\rho_a}{dt} = \sum_b m_b u_{ab} \nabla_a W_{ab} \quad (6)$$

in preference to using a weighted summation of mass terms. This is because the latter would result in an artificial density decrease as fluid interfaces are approached. As stated above, the fluid in the standard SPH formulation is considered as a weakly compressible fluid, facilitating the use of an equation of state to determine fluid pressure, which is much faster than solving an equation such as the Poissons equation. The following expresses the relationship between pressure and density by Tait's equation of state [8]:

$$P = B \left[ \left( \frac{\rho}{\rho_0} \right)^\gamma - 1 \right] \quad (7)$$

Where  $\gamma$  is 7 ,  $B$  is  $c_0^2 \rho_0 / \gamma$ ,  $\rho_0$  is 1000 kg/m<sup>3</sup> the reference density, and  $c_0$  is  $c(\rho_0)$ , the speed of sound at the reference density. The pressure gradient term in symmetrical form is expressed in SPH notation as

$$-\frac{1}{\rho} \nabla P = -\sum_b m_b \left( \frac{P_a}{\rho_a^2} + \frac{P_b}{\rho_b^2} \right) \nabla_a W_{ab} \quad (8)$$

The laminar stress term simplifies to [9]:

$$(\nu_0 \nabla^2 \vec{u}) = \sum_b m_b \left( \frac{4\nu_0 \vec{r}_{ab} \nabla_a W_{ab}}{(\rho_a + \rho_b) |\vec{r}_{ab}|^2} \right) \vec{u}_{ab} \quad (9)$$

Where  $\vec{r}_{ab} = \vec{r}_a - \vec{r}_b$ ,  $\vec{u}_{ab} = \vec{u}_a - \vec{u}_b$ ; being  $\vec{r}_k$  and  $\vec{u}_k$  the position and the velocity corresponding to particle  $k$  ( $a$  or  $b$ ) and  $\nu_0$  is the kinetic viscosity of laminar flow ( $1 \times 10^{-6} \text{ m}^2 / \text{s}$ ).

SPS is deployed to represent the effects of turbulence in Sub-Particle Scales [1]. This model improves the accuracy of SPH, owing to the fact that it preferably predicts the natural action better than the classical artificial viscosity given by Monaghan(1992) [7]. The eddy viscosity assumption is often used to model the SPS stress tensor using Favre-averaging (for a compressible fluid):

$$\frac{\tau_{ij}}{\rho} = 2\nu_t S_{ij} - \frac{2}{3} k \delta_{ij} - \frac{2}{3} C_1 \Delta^2 \delta_{ij} |S_{ij}|^2 \quad (10)$$

Where  $\tau_{ij}$  is the sub-particle stress tensor,  $\nu_t = [\min(C_s, \Delta l)]^2 |S|$  is the turbulence eddy viscosity,  $k$  is the SPS turbulence kinetic energy,  $C_s$  is the Smagorinsky constant (0.12),  $C_1 = 0.0066$ ,  $\Delta l$  is the particle-particle spacing  $|S| = (2S_{ij} S_{ij})^{1/2}$  and  $S_{ij}$  the element of SPS strain tensor. Therefore, the momentum

conservation equation can be written in SPH notation as:

$$\frac{D\vec{u}_a}{Dt} = -\sum_b m_b \left( \frac{P_a}{\rho_a^2} + \frac{P_b}{\rho_b^2} + \frac{\tau_a}{\rho_a^2} + \frac{\tau_b}{\rho_b^2} \right) \nabla_a W_{ab} + \sum_b m_b \left( \frac{4\mathbf{u}_0 \vec{r}_{ab} \cdot \nabla_a W_{ab}}{(\rho_a + \rho_b) |\vec{r}_{ab}|^2} \right) \vec{u}_{ab} + g \tag{11}$$

Kernel function has a significant role in SPH method, for analytical particles demarcate the affected area. In this study, the Quintic function is used, which is generally employed and proposed by Wendland, [10]:

$$W(r, h) = \alpha_d \left( 1 - \frac{R}{2} \right)^4 (2R + 1) \quad 0 \leq R \leq 2 \tag{12}$$

Where  $\alpha_d$  is  $7/4\pi h^2$  in 2D,  $21/16\pi h^3$  in 3D and  $R = r/h$ .

In this research, the Predictor-Corrector algorithm described by Monaghan (1989) was used in numerical simulations with a time step  $\Delta t = 5 \times 10^{-5}$  s [11]. This time step is small enough to fulfill the Courant condition and to control the stability of force and viscous terms [7].

The pressure field of the particles exhibits large pressure oscillations, although the dynamics from SPH simulations are generally realistic. Efforts have been made to overcome this problem by several approaches including correcting the kernel [12, 13] and developing an incompressible solver. One of the most straightforward and computationally least expensive methods is to apply a filter to the density of the particles and re-assign a density to each particle [14].

The Moving Least Squares (MLS) approach, which was firstly developed by (Dilts, 1999) [15] and successfully applied by Colagrossi, Landrini (2003) [14] and Panizzo (2004) [16], was used for the current modeling approach.

This is a first-order correction so that the variation of a linear density field can be exactly reproduced:

$$\rho_a^{New} = \sum_b \rho_b W_{ab}^{MLS} \frac{m_b}{\rho_b} = \sum_b m_b W_{ab}^{MLS} \tag{13}$$

The corrected kernel is evaluated as follows:

$$W_{ab}^{MLS} = W_b^{MLS}(r_a) = \beta(r_a)(r_a - r_b) W_{ab} \tag{14}$$

so that in 2-D:

$$W_{ab}^{MLS} = [\beta_0(r_a) + \beta_{1x}(r_a)(x_a - x_b) + \beta_{1z}(r_a)(z_a - z_b)] W_{ab} \tag{15}$$

where the correction vector  $\beta$  is given by

$$\beta(r_a) = \begin{pmatrix} \beta_0 \\ \beta_{1x} \\ \beta_{1z} \end{pmatrix} = A^{-1} \begin{bmatrix} 1 \\ 0 \\ 0 \end{bmatrix} \tag{16}$$

$$A = \sum_b W_b(r_a) \frac{m_b}{\rho_b} \tilde{A} \tag{17}$$

with the matrix  $\tilde{A}$  being given by

$$\tilde{A} = \begin{bmatrix} 1 & (x_a - x_b) & (z_a - z_b) \\ (x_a - x_b) & (x_a - x_b)^2 & (z_a - z_b)(x_a - x_b) \\ (z_a - z_b) & (z_a - z_b)(x_a - x_b) & (z_a - z_b)^2 \end{bmatrix} \tag{18}$$

The method is applied every 30 time steps.

### 2.2 Boundary and Initial Conditions

In the SPH model, identification and tracking of free surfaces can always be simply conducted by particles. In the computational domain no special treatment was applied on free surface particles. In fact, the main advantage of the method is that free surface is modeled naturally using the SPH method. For this modeling, the boundary is described by a set of discrete boundary particles. As described in Gómez-Gesteira and Dalrymple (2004) [17], fixed solid boundaries such as the sea bottom, a plane slope and a submerged breakwater were built with two parallel layers of fixed boundary particles set in a staggered manner. For a complete description of the mechanism refer to [18]. The upstream open boundary is the incident wave boundary. It is modeled by a numerical wave maker composed of wall particles. The wave maker moves periodically during the computation.

In this research the initial velocity of the fluid particles was considered as zero and fluid particles were initially placed on a Cartesian grid with  $dx=dz=0.008$  m. An initial density of  $\rho_0$  was assigned for particles based on hydrostatic pressure when the pressure is calculated from the equation of state. So, density of a particle (located at depth z) must be calculated taking in account the water column height as follow:

$$\rho = \rho_0 \left( 1 + \frac{\rho_0 g (H - z)}{B} \right)^{\frac{1}{\gamma}} \tag{19}$$

in which,  $H$  is the depth of the tank and  $z$  is the distance between the particle and the bottom [19].

### 2.3 Numerical Wave Flume

A 2-D non-reflection numerical wave flume is established with SPH method, and an absorbing wavemaker boundary condition and wave absorption boundary are present. The validity of the numerical model was verified through comparison of the numerical results with general wavemaker and solid boundary.

Base on linear wave-making theory, a paddle wavemaker with simple harmonic motion with amplitude  $A_p$ , and angular frequency  $\omega$ , that the equilibrium position is origin, can generate a linear wave in a flume, and the wave surface  $\eta$  is

$$\eta = A_p C_0 \cos(kx - \omega t) + A_p \sum_{n=1}^{\infty} C_n e^{-kx} \sin(\omega t) \tag{20}$$

where

$$C_0 = \frac{2[\cosh(2kh) - 1]}{\sinh(2kh) + 2kh} \quad (21)$$

$$C_n = \frac{2[\cos(2k_n h) - 1]}{\sin(2k_n h) + 2k_n h} \quad (22)$$

where  $h$  is water depth,  $x$  is the distance from wavemaker.

In this equation, the wave number  $k$  satisfies the following formula,

$$kg \cdot \tanh(kd) - \omega^2 = 0 \quad (23)$$

and  $k_n$  is the  $n$ th root of the equation below,

$$k_n g \cdot \tan(k_n d) + \omega^2 = 0 \quad (24)$$

To absorb the secondary reflecting waves from the wave maker, an additional wave maker displacement  $X_a$  is added on the original displacement  $X_p$ . Then, the displacement of the absorbing wavemaker is

$$X = X_p + X_a = A_p \sin(\alpha t) + A_a \sin(\alpha t + \varphi) \quad (25)$$

The final expression of the velocity of the paddle can be obtained as

$$u(t) = \frac{dX}{dt} = \frac{\omega}{C_0} [2\eta_p - \eta_m + D \cdot X(t)] \quad (26)$$

where  $\varphi$  is phase difference,  $\eta_p$  is the wave surface generated by  $X_p$ ,  $\eta_m$  is the wave surface that

measured in front of the wave maker, and  $D = \sum_{n=1}^{\infty} C_n$  [20].

To absorb the wave reflection from the wall at the end of the open channel, an exponential damping zone is placed over a distance of at least a wavelength. In the damping zone, the velocity of fluid particles will be damped as

$$U = U_0 [1 - \exp(-\alpha(\delta x_0 - (x - x_0)))] \quad (27)$$

where  $U$  is fluid velocity,  $\alpha$  is a coefficient, equal to 2.0;  $\delta x_0$  is the damping zone length,  $x_0$  is the damping zone starting point,  $x_0 = L - \delta x_0$  and  $L$  is the channel length [4].

### 3.0 VALIDATION

In order to verify the capacity of absorbing secondary reflecting waves from the wavemaker in numerical wave tank, the layout of an example is shown in Figure 1. The incident regular wave height is 0.08m, period is 1.5 s and solid wall is set as the right boundary of the flume.

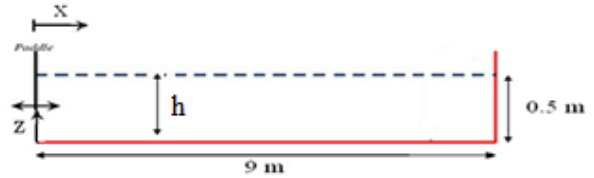


Figure 1 Layout of computational domain

To verify the capacity of absorbing secondary reflecting waves from the wavemaker in numerical wave tank using SPH method, the variations of the wave surface at different locations of the wave tank were compared with the values of a general wave maker.

Figure 2 shows the time series of the wave surface at different monitoring points in the wave flume generated by absorbing wavemaker and general wavemaker. The figure shows that the time series of the wave surface at the monitoring points with the absorptive wave maker keep stable. The reflecting waves from flume is absorbed by the absorptive wavemaker, and stationary wave superposed by incident wave and reflected wave from the end wall can be observed. The wave height of the stationary wave is 2 times of the incident one. But at node points ( $x = 6.68\text{m}$ ), the wave height is small. However, the second reflecting waves from the wavemaker are obvious at the monitoring points by using the general wavemaker, and the wave height is increasing gradually. At node points, the variation of wave surface is greater and makes the variation of wave shape unstable.

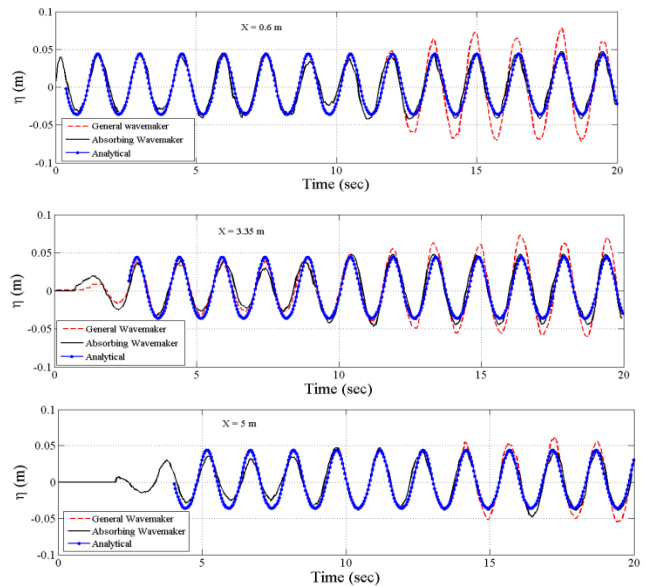


Figure 2 Comparison of wave surface with absorbing wavemaker and general wavemaker at different monitoring points in the flume

To verify the absorbing properties of the sponge layer, a sponge layer is set before the end of the wave flume. Figure 3 shows the layout of the computational domain, in which the incident regular wave height is 0.09m, period is 1.2s and the length of the damping zone is 3 m (i.e., about 1.5 times of the wave length).

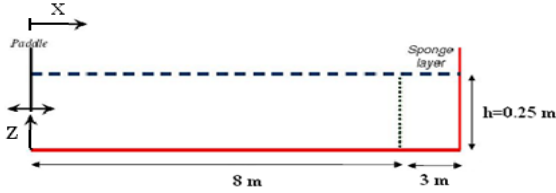


Figure 3 Layout of computational domain

Figure 4 shows the time series of the wave surface at different monitoring points in the wave flume. This figure indicates that the waves can be effectively absorbed using the defined sponge layer.

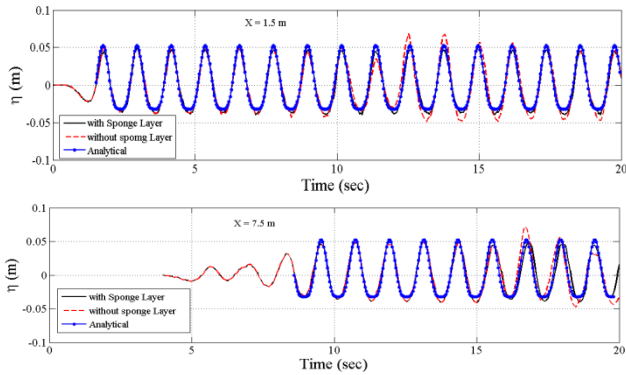


Figure 4 Comparison of wave surface with and without sponge layer at different monitoring points in the flume

In order to verify the performance of the developed numerical wave flume, the laboratory experimental results of Mahmoudi (2014) was used [21]. Figure 3 shows general layout and important parameters of their experimental work. A regular wave with a height  $H = 0.067$  m and period  $T = 1.2$  sec was used.

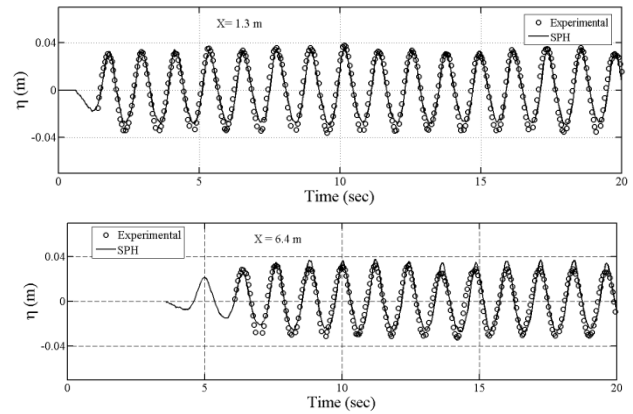


Figure 5 Comparison of computed water surface elevations by SPH with experimental data at different monitoring points in the flume

The observed differences between the numerical and experimental results can be quantified by means of two statistical parameters.

$$P_d = \left( \frac{\sum_i (\text{Var}_i^{\text{num}} - \text{Var}_i^{\text{exp}})^2}{\sum_j (\text{Var}_j^{\text{exp}})^2} \right)^{1/2} \quad (28)$$

$$A_r = \left( \frac{\sum_i (\text{Var}_i^{\text{num}})^2}{\sum_j (\text{Var}_j^{\text{exp}})^2} \right)^{1/2} \quad (29)$$

where "Var" is the variable that has to be considered and the superscripts refer to experimental or numerical values. The first parameter,  $A_r$ , represents the relative amplitude of both signals, in such a way that a perfect agreement between the experimental and numerical data would result in  $A_r \rightarrow 1$ . On the other hand, the second parameter,  $P_d$ , is the phase difference between both signals, a perfect agreement would result in  $P_d \rightarrow 0$ .

Table 1 summarizes the values of  $A_r$  and  $P_d$  obtained for the WCSPH (present model) and experimental data of Mahmoudi (2014). Both statistical parameters show a satisfactory agreement between the numerical and experimental solutions.

Table 1 Statistical parameters  $A_r$  and  $P_d$  for the WCSPH (present model) and experimental data of Mahmoudi (2014)

	x=1.3 m	x=6.4 m
$A_r$	0.952	1.051
$P_d$	0.643	0.351
RMSE	0.014	0.0095

In this paper, in order to validate the developed numerical model, other experimental data set was used.

### 3.1 Wave Propagation over Impermeable Trapezoidal Sea Wall

In order to simulate the periodic wave propagation over impermeable trapezoidal sea wall on plane bed, the laboratory experimental results of Li *et al.* (2004) was used [22]. Figure 6 shows general layout and important parameters of their experimental work. The computational domain covering a sea wall was 6.3 m long and 1.0 m high. A regular wave with a height  $H = 0.16$  m and period  $T = 2.0$  sec was used.

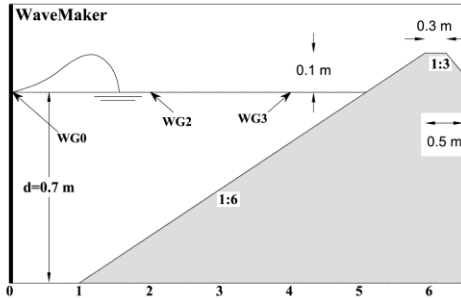


**Figure 6** Schematic of the numerical flume and sloping sea wall for wave breaking [22]

The WCSPH approach with LES modeling was used to investigate regular wave propagation over a smooth impermeable sea wall. For a quantitative evaluation of the SPH computations with LES modeling, the computed water surface elevations at two gauging stations are shown in Figures 7 and 8. The experimental and numerical data of Li *et al.* [22] are also included in the figures. Li *et al.* used a time-implicit cell-staggered approximately factored VOF finite volume approach for solving the unsteady incompressible N-S equations based on the non-uniform Cartesian cut-cell grids. Meanwhile, the effects of turbulence were addressed by using both static and dynamic sub-grid scale (SGS) LES turbulence models in their formulations. As shown in Figures 7 and 8, WCSPH results are better agree with experimental data than those of Li *et al.* [22]. This good agreement is mainly attributed to the fact that the free surface is accurately tracked by the particles without numerical diffusion in the SPH approach.

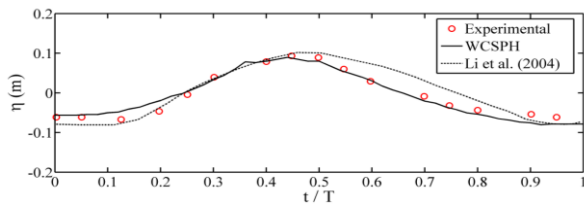


**Figure 7** Comparison of computed water surface elevations by SPH with experimental and numerical data of Li *et al.* [22] for WG2 ( $x=2.02$  m)

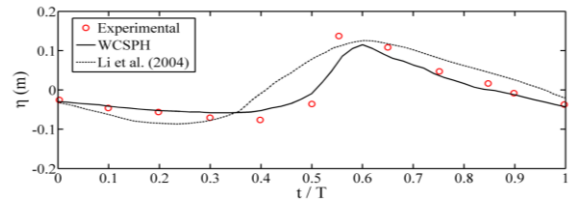


**Figure 8** Comparison of computed water surface elevations by SPH with experimental and numerical data of Li *et al.* [22] for WG3 ( $x=3.81$  m)

Table 2 summarizes the values of  $A_r$  and  $P_d$  obtained for the WCSPH (present model) and numerical data of Li *et al.* [22]. Although both statistical parameters show a satisfactory agreement between the numerical and experimental solutions, however, the numerical model results show to be more accurate when using the WCSPH method.

**Table 2** Statistical parameters  $A_r$  and  $P_d$  for the WCSPH (present model) and numerical data of Li *et al.* [22]

	SPH method		Li <i>et al.</i> (2004)	
	for WG2 ( $x=2.02$ m)	for WG3 ( $x=3.81$ m)	for WG2 ( $x=2.02$ m)	for WG3 ( $x=3.81$ m)
$A_r$	0.986	0.93	1.183	1.098
$P_d$	0.1698	0.215	0.3796	0.658

### 4.0 CONCLUSION

This paper established a numerical wave flume with SPH method. An absorbing wavemaker and a damping zone are set in the model to eliminate the influence of secondary reflecting waves from the wave maker and to absorb the incoming waves at the end of flume. The comparison of the numerical model results and the ordinary numerical model wave maker and solid wall boundary shows that the model can absorb waves efficaciously, and this provides a basic program for the study on the interaction between waves and structures.

### References

- [1] Dalrymple, R. A., Rogers, B. D. 2006. Numerical Modeling Of Water Waves With The SPH Method. *Coastal Engineering*, 53: 141-147.
- [2] Liu, Q. H., Zhao, Z. D. 1999. Numerical Wave Flume And Its Verification. *Journal of Hydrodynamics, Ser A*, 14(1): 8-15.
- [3] Shi Ruixiang, Zhou Zongren, Yin Zhang. 2004. Numerical Study On A Two Dimensional Numerical Wave Tank With Its Application In The Generation And Propagation Of Irregular Waves. *Journal of Yanshan University*, 28(2): 172-178.
- [4] Xu, R. 2010. An Improved Incompressible Smoothed Particle Hydrodynamics Method And Its Application In Free-Surface Simulations. PhD Dissertation, University of Manchester, UK.
- [5] Omidvar, P., Stansby, P. K., Rogers, B. D. 2012. Wave Body Interaction In 2D Using Smoothed Particle Hydrodynamics (SPH) With Variable Particle Mass. *International Journal for Numerical Methods in Fluids*, 68: 686-705.

- [6] Delavari, E., Mostafa Gharabaghi, A. R. 2014. A Modified Sponge Layer Boundary Condition For A Numerical Wave Flume Based On The SPH Scheme. *The 11<sup>th</sup> International Conference on Coasts, Ports and Marine Structures (ICOPMAS 2014)*, Tehran, Iran.
- [7] Monaghan, J. J. 1992. Smoothed Particle Hydrodynamics. *Annual Review Of Astronomy And Astrophysics*. 30: 543-574.
- [8] Monaghan, J. J. 1994. Simulating Free Surface Flows With SPH. *Journal Computational Physics*. 110: 399-406.
- [9] Lo, E., Shao, S. 2002. Simulation Of Near-Shore Solitary Waves Mechanics By An Incompressible SPH Method. *Applied Ocean Research*. 24: 275-286.
- [10] Wendland, H. 1995. Piecewise Polynomial, Positive Definite And Compactly Supported Radial Functions Of Minimal Degree. *Advances In Computational Mathematics*. 4: 389-396.
- [11] Monaghan, J. J. 1989. On The Problem Of Penetration In Particle Methods. *Journal of Computational Physics*. 82: 1-15.
- [12] Bonet, J., Lok, T. S. 1999. Variational And Momentum Preservation Aspects Of Smooth Particle Hydrodynamic Formulation. *Computer Methods in Applied Mechanics and Engineering*. 180: 97-115.
- [13] Bonet, J., Kulasegaram, S. 2000. Correction And Stabilization Of Smooth Particle Hydrodynamic Methods With Applications In Metal Forming Simulations. *International Journal for Numerical Methods in Engineering*. 47: 1189-1214.
- [14] Colagrossi, A., Landrini, M. 2003. Numerical Simulation Of Interfacial Flows By Smoothed Particle Hydrodynamics. *Journal of Computational Physics*. 191: 448-475.
- [15] Dilts, G. A. 1999. Moving-LeastSquares-Particle Hydrodynamics I, Consistency and stability. *International Journal for Numerical Methods in Engineering*. 44: 1115-1155.
- [16] Panizzo, A. 2004. Physical and Numerical Modelling of Sub-aerial Landslide Generated Waves. PhD thesis, UniversitadegliStudi di L'Aquila.
- [17] Gomez-Gesteira, M., Dalrymple, R. A. 2004. Using a Three Dimensional Smoothed Particle Hydrodynamics Method for Wave Impact on a Tall Structure. *Journal of Waterway Port Coastal and Ocean Engineering*. 130(2).
- [18] Crespo, A. J. C., Gomez-Gesteira, M., Dalrymple, R. A. 2007. 3D SPH Simulation Of Large Waves Mitigation With A Dike. *Journal of Hydraulic Research*. 45(5): 631-642.
- [19] Gomez-Gesteira, M., Cerqueiro, D., Crespo, C., Dalrymple, R. A. 2005. Green Water Overtopping Analyzed With A SPH Model. *Ocean Engineering*. 32: 223-238.
- [20] Liu, S. X., Wang, X. T., Li, M. G., Guo, M. Y. 2003. Active Absorption Wave Maker System For Irregular Waves. *China Ocean Engineering*. 17(2): 203-214.
- [21] Mahmoudi, A. 2014. Development of the Modified Smoothed Particle Hydrodynamic Model to Investigate the Performance of a Trapezoidal Submerged Breakwater. PhD Thesis, Sahand University of Technology, Tabriz, Iran.
- [22] Li, T.Q., Troch, P., Rouck J. D. 2004. Wave Overtopping Over A Sea Dyke. *Journal of Computational Physics*. 198: 686-7.